

A Fortescue Approach for Real-Time Short Circuit Computation in Multiphase Distribution Networks

Rabih A. Jabr, *Senior Member, IEEE*, and Izudin Džafić, *Senior Member, IEEE*

Abstract—This paper discusses the need for short circuit analysis in real-time applications of modern distribution networks and presents a short circuit tool that builds on recent advances in Fortescue-based current injection power flow. The proposed short circuit computation (SCC) method is fundamentally based on the symmetrical components transformation of three-phase, two-phase, and one-phase systems. Unlike the classical symmetrical components SCC method that postulates a structurally symmetrical three-phase pre-fault network with balanced loading, the proposed method accounts for multiphase networks that are comprised of three-phase, two-phase, and one-phase network parts; given a pre-fault power flow solution, it requires a maximum of three current injection iterations to compute the short circuit current flow in the entire network. Numerical results show that the Fortescue SCC approach with multiphase lines exhibits significant computational performance improvement on large-scale networks as compared to classical SCC in phase coordinates.

Index Terms—Distribution networks, fault analysis, Fortescue transformation, symmetrical components.

I. INTRODUCTION

THE analysis of faulted transmission power systems is classically carried out using the theory of symmetrical components [1]. Symmetrical components is an elegant method which was published by Fortescue in 1918 [2], and its main advantage is well known: when a three-phase network is symmetrical, the corresponding sequence networks are uncoupled thus leading to reduced computational effort. Additionally, the generator and transformer modeling in terms of symmetrical components is relatively simple, and the power component data is usually available in terms of sequence values. Short circuit computation (SCC) is a real-time application in modern distribution networks [3], [4]; it is employed for the identification of fault locations and for performing checks on the protection system, possibly involving an update of relay settings, prior to implementing feeder reconfiguration.

The classical application of symmetrical components to SCC is based on the premise that the normal pre-fault network is symmetrical and with balanced loads; while this assumption is ac-

ceptable at the transmission level, it does not hold in many distribution system feeders where the number of phases is less than three. In a two-part paper published in 1968 [5], [6], Laughton introduced the method of phase coordinates to deal with the peculiarities of distribution system representation and fault analysis. For SCC, Laughton discussed two approaches. The first approach is the distributed-source method; it is referred to as such because the various sources and power components retain their identity during fault computation, which resorts to standard linear algebra methods for solving systems of linear equations. The second approach is based on source superposition; this method operates by first determining the fault current using a Thévenin (or Norton) network representation, and then computing the bus voltages by superposition of the pre-fault voltages on the voltage drops due to the fault currents acting alone. There have been several more recent and notable contributions that also make use of fault analysis in phase coordinates, for instance, the canonical model in [7] and Kersting's approach [8]–[10]; both of these methods employ source superposition, which has emerged as the more popular alternative in comparison with the distributed-source methods particularly due to computational advantages. The Generalized Distribution Analysis System [4], also based on superposition, is oriented towards applications in distribution system operation by employing the unity current injection method for computing both the Thévenin impedance matrix and the post-fault voltage vector. Nevertheless, the distributed-source method was also investigated in [11], where it was argued that the effect of modeling metallic (zero impedance) faults using small resistances could result in calculation errors; the accurate solution is along the lines originally proposed in [6] and involves solving the normal system of equations subject to a number of boundary constraints, which is also equivalent to modifying the nodal admittance matrix to obtain a number of reduced equations for solution without constraints. Another technique [12] involves the use of a continuation method with the three-phase current injection power flow [13]; in this case, the continuation parameter is the fault impedance which is decreased in steps to reach the desired value while ensuring convergence of the power flow solution. The continuation method is however likely to be computationally prohibitive for real-time fault analysis.

In an effort to further improve computational performance, fault analysis programs were built around the backward-forward sweep (BFS) solver as opposed to power flow that uses the network nodal admittance matrix. The BFS solver is ideally suited for radial distribution networks, in which case it is known to be more efficient than the current injection method. An efficient three-phase power flow implementation of BFS was introduced

Manuscript received June 14, 2014; revised October 14, 2014; accepted November 25, 2014. Date of publication December 18, 2014; date of current version August 03, 2015. Paper no. TPWRS-00810-2014.

R. A. Jabr is with the Department of Electrical and Computer Engineering, American University of Beirut, Riad El—Solh/Beirut 1107 2020, Lebanon (e-mail: rabih.jabr@aub.edu.lb).

I. Džafić is with the International University of Sarajevo, 71210 Sarajevo, Bosnia (e-mail: idzafic@iee.org).

Color versions of one or more of the figures in this paper are available online at <http://ieeexplore.ieee.org>.

Digital Object Identifier 10.1109/TPWRS.2014.2376198

in [14]; it makes use of a multi-port compensation technique to handle PV nodes and meshed distribution networks. Reference [3] extended the compensation technique in [14] to additionally include fault representations. Alternative approaches for fault analysis, which are similar to forward-backward sweep techniques, have been proposed in [15]–[17]. Fault computation makes use of the widely accepted three-phase line section in which the neutral wire is eliminated using Kron reduction [8], based on the practical assumption that the grounding impedance is small. However, the surveyed SCC approaches are also applicable to four-wire distribution networks, as demonstrated for instance in [18].

Contrary to common perception, this paper shows that there is a computational performance advantage when using the symmetrical components approach for fault analysis of multiphase distribution networks. This is of importance given the real-time nature of the SCC application. [19] has recently shown that single-phase and two-phase distribution feeders can be represented in an equivalent three-phase radial and symmetrical distribution system having uncoupled sequence networks, but this entails an approximation error for two-phase line segments. This paper demonstrates that SCC of multiphase distribution networks, which are possibly meshed, can be accurately performed using symmetrical components; the multiphase network is comprised of three-phase, two-phase, and one-phase network parts, which is representative of typical distribution networks. The proposed SCC is built around a Fortescue implementation of the current injection method applied to multiphase distribution networks, where it was demonstrated that there is significant computational improvement relative to performing computations in phase coordinates [20]. The major computational burden in the proposed Fortescue SCC is attributed to one LU factorization of the Fortescue nodal admittance matrix and a number of forward/backward solutions equal to the number of phases in the faulted node, which can be one, two, or three; the factorization remains valid as long as the pre-fault network conditions are unchanged. The SCC computation produces all node voltages, branch currents, and fault currents at the short circuit location. This paper presents contributions beyond the implicit Z-bus power flow in Fortescue coordinates [20]: 1) a general model for any fault type in multiphase distribution networks using Fortescue coordinates, 2) a general procedure for SCC in multiphase distribution networks using Fortescue coordinates, involving the use of a generalized Fortescue Thévenin equivalent.

The rest of this paper is organized as follows. Section II motivates the need for real-time SCC in modern distribution networks, particularly for the computation of the circuit breaker maximal and minimal currents. The computational engine behind the SCC approach is the Fortescue equivalent nodal admittance matrix approach to power flow solution [20], which is reviewed in Section III. Section IV introduces the Fortescue SCC in multiphase networks, and Section V presents the boundary conditions for short circuit modeling of multiphase nodes; a demonstration example of the procedure is given in Section VI. Numerical results in Section VII serve to establish the validity of the Fortescue SCC by comparing with the classical canonical approach in phase coordinates [4], [7]; additionally, Section VII reports computational performance

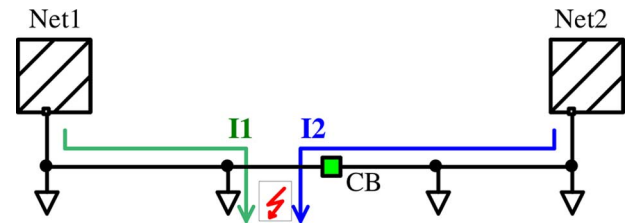


Fig. 1. Fault on the left side of the circuit breaker.

comparisons on large-scale SCC instances. The paper is concluded in Section VIII.

II. MOTIVATION: SHORT CIRCUIT CALCULATION SCREENING

In the real-time operation of distribution networks, SCC is carried out at multiple fault locations. Each location, representing a node in the network area, is considered separately. The standard short circuit types which are available for real-time SCC screening are: 1) single line-to-ground (SLG) fault, 2) line-to-line (LL) fault, 3) double line-to-ground (2LG) fault, 4) three-phase (3-ph) fault without ground connection, and 5) three-phase to ground (3-ph-G) fault. The results for 3-ph and 3-ph-G faults will be identical only in the case of a structurally symmetrical network with balanced loading, which is not a typical model in practical distribution systems. SCC screening is normally carried out automatically, either on a cyclical basis or following a request for topology change; it is used to check for violations of circuit breaker/fuse breaking capability, to check the adequacy of the relay sensitivity, and to check the levels of earth fault currents. These three checks are discussed in the sections below.

A. Checking of the Circuit Breaker/Fuse Breaking Capability

Each circuit breaker (CB) or fuse in the network is checked for the maximum current that can flow through it under the worst case fault condition; this condition is referred to as the maximal current mode. A fault is therefore simulated at each CB (or fuse) location to check if the corresponding CB breaking capacity is violated. The 3-ph-G fault is often the most severe, however an exception is the SLG fault at the Y-grounded side of a Δ -Y transformer bank [1]; the appropriate fault type has to be chosen at each CB location. Consider for illustration a fault simulated to the left (Fig. 1) or to the right (Fig. 2) of a CB. The current flowing through the fault is the same in both figures because the CB ideally has zero impedance; this implies that the short circuit computation has to be carried out only once. However, the actual line current flowing through the breaker can generally be different depending on whether the fault is on the left of the CB where the CB current is supplied by Network 2, or on its right where the CB current is from Network 1. The critical CB current is therefore the maximum of the two values identified in Figs. 1 and 2. When the CB is in a radial part of the network, i.e., supplied from only one side, the critical CB current will be the same as the short circuit current at the CB location. In any case, whenever the CB current is greater than the CB breaking capacity, the CB is flagged as violated. If the CB current is close to but slightly less than the breaking capacity, then the CB is flagged as suspicious.

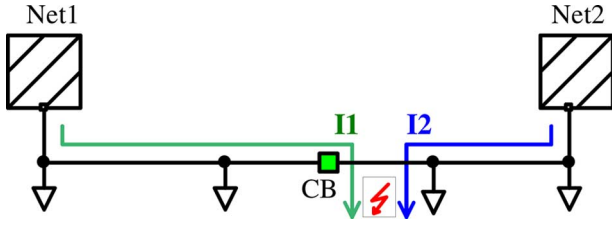


Fig. 2. Fault on the right side of the circuit breaker.

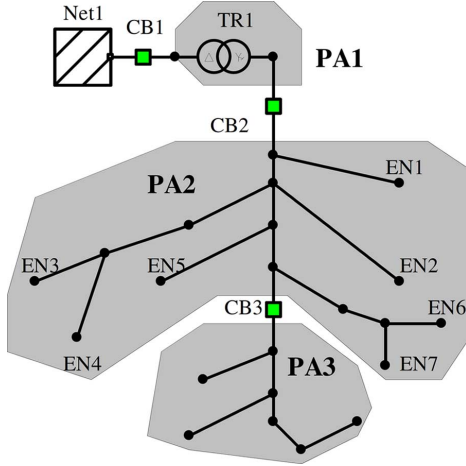


Fig. 3. Protection areas and end nodes in protection area 2.

B. Checking of the Relay Sensitivity

Unlike the maximal current mode, checking of the relay sensitivity involves computing the minimum short circuit current through the breaker and comparing it with the relay setting. In this computation, which is referred to as the minimal current mode, the CB is flagged as violated if the minimum short circuit current through it is less than the relay setting value. For a particular CB, the critical nodes in the minimal current mode are the ones that are covered by the CB and at which a fault can potentially produce the minimum current through this CB. For example, in Fig. 3, the leaf nodes EN1 through EN7 are the critical buses for CB2; the fault types for minimal current mode are commonly chosen as LL for ungrounded networks (fed from the transformer Δ -side) and as SLG or 2LG for grounded networks.

C. Checking of the Ground Fault Current

Safety regulations limit the maximum ground fault current at a fault location. The ground current is compared to a pre-specified limit, which itself depends on the busbar voltage level and the network grounding type. If the current limit is exceeded, then the node at which the fault is simulated is flagged as violated with respect to the earth current limit. Checking the ground fault current at the different nodes spans the following fault types: SLG, 2LG, and 3-ph-G.

III. FORTESCUE EQUIVALENT NODAL ADMITTANCE MATRIX

Recent research has shown a practical advantage of applying the symmetrical components method to the power flow solution of multiphase distribution systems that contain three-phase, two-phase, and one-phase network parts [20], [21]. In particular, [20] shows performance improvement of the Current Injection

(CI) method when computations are carried out in Fortescue coordinates as opposed to phase coordinates. Consider for illustration a symmetrical three-phase line having the ordinary primitive admittance matrix:

$$\underline{Y}_{ph3} = \begin{bmatrix} \underline{y}_s & \underline{y}_m & \underline{y}_m \\ \underline{y}_m & \underline{y}_s & \underline{y}_m \\ \underline{y}_m & \underline{y}_m & \underline{y}_s \end{bmatrix} \quad (1)$$

where the underlined quantities take complex values. It is well known that (1) can be transformed into the Fortescue domain of order 3 (F_3), resulting in a diagonal matrix [1]:

$$\begin{aligned} \underline{Y}_{F_3} &= \underline{T}_{ph3}^{F_3} \underline{Y}_{ph3} \underline{T}_{F_3}^{ph3} \\ &= \begin{bmatrix} \underline{y}_s + 2\underline{y}_m & 0 & 0 \\ 0 & \underline{y}_s - \underline{y}_m & 0 \\ 0 & 0 & \underline{y}_s - \underline{y}_m \end{bmatrix} \end{aligned} \quad (2)$$

where

$$\underline{T}_{F_3}^{ph3} = \begin{bmatrix} 1 & 1 & 1 \\ 1 & \underline{a}_3^2 & \underline{a}_3 \\ 1 & \underline{a}_3 & \underline{a}_3^2 \end{bmatrix}; \quad \underline{T}_{ph3}^{F_3} = (\underline{T}_{F_3}^{ph3})^{-1}; \quad \underline{a}_3 = e^{j2\pi/3}. \quad (3)$$

Similar equations are applicable to a symmetrical two-phase line in the Fortescue domain of order 2 (F_2) [20]:

$$\underline{Y}_{ph2} = \begin{bmatrix} \underline{y}_s & \underline{y}_m \\ \underline{y}_m & \underline{y}_s \end{bmatrix} \quad (4)$$

$$\underline{Y}_{F_2} = \underline{T}_{ph2}^{F_2} \underline{Y}_{ph2} \underline{T}_{F_2}^{ph2} = \begin{bmatrix} \underline{y}_s + \underline{y}_m & 0 \\ 0 & \underline{y}_s - \underline{y}_m \end{bmatrix} \quad (5)$$

$$\begin{aligned} \underline{T}_{F_2}^{ph2} &= \begin{bmatrix} 1 & 1 \\ 1 & \underline{a}_2 \end{bmatrix}; \quad \underline{T}_{ph2}^{F_2} = (\underline{T}_{F_2}^{ph2})^{-1}; \\ \underline{a}_2 &= e^{j2\pi/2} = -1. \end{aligned} \quad (6)$$

For a one-phase line, the ordinary primitive admittance matrix representations in phase and Fortescue coordinates are identical:

$$\underline{Y}_{ph1} = \underline{y}_s \quad (7)$$

$$\underline{Y}_{F_1} = \underline{T}_{ph1}^{F_1} \underline{Y}_{ph1} \underline{T}_{F_1}^{ph1} = \underline{y}_s \quad (8)$$

$$\underline{T}_{F_1}^{ph1} = e^{j2\pi} = 1; \quad \underline{T}_{ph1}^{F_1} = (\underline{T}_{F_1}^{ph1})^{-1} = 1. \quad (9)$$

The formation of the network nodal admittance (\underline{Y}_{node}) matrix can be easily performed firstly by computing the primitive \underline{Y}_{node} matrices for each of the network components, and secondly by overlapping them together [22]. For example, the primitive \underline{Y}_{node} matrix corresponding to the symmetrical two-phase line in the Fortescue domain (5) is the 4×4 matrix:

$$\underline{Y}_{node}^{F_2} = \begin{bmatrix} \underline{Y}_{F_2} & -\underline{Y}_{F_2} \\ -\underline{Y}_{F_2} & \underline{Y}_{F_2} \end{bmatrix}. \quad (10)$$

Now assume that the formation of the network \underline{Y}_{node} matrix requires overlapping the primitive \underline{Y}_{node} matrix of the two-phase line given by (10) between two nodes i and j of the partial network \underline{Y}_{node} matrix formed so far. If both nodes i and j are of the two-phase type, then the network overlapping [22] is straightforward. However, if node i is of the three-phase type and node j is of the two phase-type, then a special transformation is needed to convert (10) into a 5×5 matrix before network overlapping could be carried out. Reference [20] refers to nodes that connect

circuit elements with different numbers of phases as phase transition nodes (PTNs), and presents generalized primitive \underline{Y}_{node} matrices in the Fortescue domain for laterals that are commonly drawn from three-phase feeders: 1) three-phase to two-phase lateral, which is the case discussed above, 2) three-phase to single-phase lateral, and 3) two-phase to single-phase lateral. With the technique in [20] for handling PTNs, the nodal network equations in the Fortescue domain can be written as

$$\begin{bmatrix} I_{11}^F & 0 & \cdots & 0 & \cdots & 0 \\ \underline{Y}_{21}^F & \underline{Y}_{22}^F & \cdots & \underline{Y}_{2i}^F & \cdots & \underline{Y}_{2N}^F \\ \vdots & \vdots & & \vdots & & \vdots \\ \underline{Y}_{i1}^F & \underline{Y}_{i2}^F & \cdots & \underline{Y}_{ii}^F & \cdots & \underline{Y}_{iN}^F \\ \vdots & \vdots & & \vdots & & \vdots \\ \underline{Y}_{N1}^F & \underline{Y}_{N2}^F & \cdots & \underline{Y}_{Ni}^F & \cdots & \underline{Y}_{NN}^F \end{bmatrix} \begin{bmatrix} \underline{V}_1^F \\ \underline{V}_2^F \\ \vdots \\ \underline{V}_i^F \\ \vdots \\ \underline{V}_N^F \end{bmatrix} = \begin{bmatrix} \underline{V}_s^F \\ \underline{I}_2^F \\ \vdots \\ \underline{I}_i^F \\ \vdots \\ \underline{I}_N^F \end{bmatrix}. \quad (11)$$

In (11), \underline{I}_i^F denotes the Fortescue injection current at node i ; its size is 3×1 , 2×1 , or 1×1 depending on whether the node is three-phase (F_3), two-phase (F_2), or single-phase (F_1):

$$\underline{I}_i^{F_3} = \begin{bmatrix} \underline{I}_i^0 \\ \underline{I}_i^1 \\ \underline{I}_i^2 \end{bmatrix}; \underline{I}_i^{F_2} = \begin{bmatrix} \underline{I}_i^0 \\ \underline{I}_i^1 \end{bmatrix}; \underline{I}_i^{F_1} = [\underline{I}_i^0]. \quad (12)$$

A similar interpretation applies to the Fortescue voltage at node i , \underline{V}_i^F . The first row in (11) sets the voltage at the slack node (number 1) to a pre-specified value; I_{11}^F is typically a 3×3 identity matrix for a three-phase slack node and $\underline{V}_s^F = \underline{V}_s^{F_3} = [0; \underline{V}_s; 0]^T$, where \underline{V}_s is the positive sequence slack voltage. Rows 2 to N in the Fortescue nodal admittance matrix (11) are obtained by network overlapping. With the loads specified in terms of their complex power, the power flow problem can be solved starting from (11) by using the CI method [20].

In fault simulations however, voltage levels fall well below the nominal range and loads switch to constant impedance models [1], [4]. Starting from the complex power consumption, the three-phase, two-phase, and one-phase loads are converted to admittances at nominal voltage (or the voltage from the distribution system power flow results) and then transformed into the Fortescue domain—similar to the development in (2), (5), and (8). The loads therefore become circuit elements that are included in the Fortescue nodal admittance matrix on the left hand side of (11), and all load current injections on the right hand side of (11) are set to zero. With the constant impedance load model, the CI method converges in one iteration.

IV. FORTESCUE SHORT CIRCUIT COMPUTATION

The short circuit computation is associated with a structural network change at the faulted node k . The structural change represents either a balanced or an unbalanced condition at node k ; the conditions can be captured by the boundary equations expressed in terms of phase coordinates using (13) for a three-phase faulted node, (14) for a two-phase faulted node, and (15) for a one-phase faulted node:

$$\underline{C}_{I3\phi} \underline{I}_k^{ph_3} + C_{V3\phi} \underline{V}_k^{ph_3} = 0; ph_3 = abc \quad (13)$$

$$\underline{C}_{I2\phi} \underline{I}_k^{ph_2} + C_{V2\phi} \underline{V}_k^{ph_2} = 0; ph_2 \in \{ab, bc, ca\} \quad (14)$$

$$\underline{C}_{I1\phi} \underline{I}_k^{ph_1} + C_{V1\phi} \underline{V}_k^{ph_1} = 0; ph_1 \in \{a, b, c\}. \quad (15)$$

The matrices ($\underline{C}_{I3\phi}$, $C_{V3\phi}$, $\underline{C}_{I2\phi}$, $C_{V2\phi}$, $\underline{C}_{I1\phi}$, $C_{V1\phi}$) that define the boundary conditions are listed in Section V for standard fault types. Equations (13)–(15) are easily expressed in terms of Fortescue coordinates as follows:

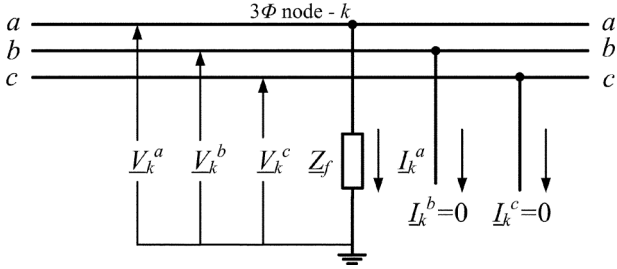
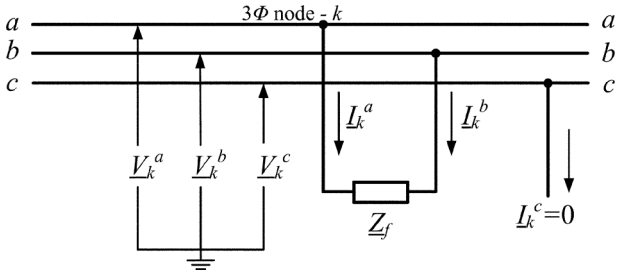
$$[\underline{C}_{I3\phi} T_{F_3}^{ph_3}] \underline{I}_k^{F_3} + [C_{V3\phi} T_{F_3}^{ph_3}] \underline{V}_k^{F_3} = 0 \quad (16)$$

$$[\underline{C}_{I2\phi} T_{F_2}^{ph_2}] \underline{I}_k^{F_2} + [C_{V2\phi} T_{F_2}^{ph_2}] \underline{V}_k^{F_2} = 0 \quad (17)$$

$$[\underline{C}_{I1\phi} T_{F_1}^{ph_1}] \underline{I}_k^{F_1} + [C_{V1\phi} T_{F_1}^{ph_1}] \underline{V}_k^{F_1} = 0. \quad (18)$$

The Fortescue voltages and currents at the faulted node can be computed by combining the boundary conditions in the Fortescue domain (16)–(18) with the Thévenin equivalent model at this point. If the Fortescue voltages at all nodes of the faulted network are desired, they can be obtained by superimposing on the pre-fault voltages the voltage changes that are attributed to the injection of the Fortescue fault currents at the faulted node; as shown below, this computation can be efficiently done using network linearity, i.e., by simply scaling the solution vectors already obtained in the Thévenin impedance calculation. Then the Fortescue currents in any branch can be computed from the branch model [20] and the obtained Fortescue node voltages, followed by the use of the synthesis equations to give the branch phase currents at that location. The procedure for SCC is as follows:

- Step 1) Read the network data and the load data. Convert the the multiphase loads into their constant impedance models at nominal voltage and form the load and branch models in the Fortescue domain [20]; this translates into setting all the injection currents \underline{I}_i^F which represent load on the right-hand side of (11) to zero. Factorize the coefficient matrix on the left hand side of (11) using LU decomposition: $\underline{Y}^F = \underline{Y}_L^F \underline{Y}_U^F$ [23]. The network nodes are ordered so as to minimize fill-in in the LU factors.
- Step 2) Solve the nodal network equations in the Fortescue domain (11) using forward/backward substitution [23] to obtain the Fortescue pre-fault voltage vector, also referred to as the Thévenin voltage vector \underline{V}_{Th}^F . If k is the index of the node to be faulted, then the Fortescue pre-fault voltages at this node are denoted by the Thévenin node voltage vector: $\underline{V}_{Th-k}^{F_3}$ for a three-phase node, $\underline{V}_{Th-k}^{F_2}$ for a two-phase node, and $\underline{V}_{Th-k}^{F_1}$ for a one-phase node.
- Step 3) Calculate the Fortescue Thévenin impedance matrix at the faulted node by deactivating all sources and injecting a unity current, one at a time, at each of the phases of the Fortescue node. The Thévenin impedance matrix computation requires performing a number of forward/backward substitutions equal to the number of phases of the faulted node.

Fig. 4. SLG fault at phase a of a three-phase node.Fig. 5. LL fault between phases a - b of a three-phase node.

- Three-phase fault node k

$$\underline{Y}_L^F \underline{Y}_U^F \begin{bmatrix} \underline{Z}_{1k}^{00} & \underline{Z}_{1k}^{01} & \underline{Z}_{1k}^{02} \\ \vdots & \vdots & \vdots \\ \underline{Z}_{kk}^{00} & \underline{Z}_{kk}^{01} & \underline{Z}_{kk}^{02} \\ \underline{Z}_{kk}^{10} & \underline{Z}_{kk}^{11} & \underline{Z}_{kk}^{12} \\ \underline{Z}_{kk}^{20} & \underline{Z}_{kk}^{21} & \underline{Z}_{kk}^{22} \\ \vdots & \vdots & \vdots \\ \vdots & \vdots & \vdots \end{bmatrix} = \begin{bmatrix} 0 & 0 & 0 \\ \vdots & \vdots & \vdots \\ 1 & 0 & 0 \\ 0 & 1 & 0 \\ 0 & 0 & 1 \\ \vdots & \vdots & \vdots \\ 0 & 0 & 0 \end{bmatrix} \quad (19)$$

$$\Rightarrow \underline{Z}_{Th-k}^{F_3} = \begin{bmatrix} \underline{Z}_{kk}^{00} & \underline{Z}_{kk}^{01} & \underline{Z}_{kk}^{02} \\ \underline{Z}_{kk}^{10} & \underline{Z}_{kk}^{11} & \underline{Z}_{kk}^{12} \\ \underline{Z}_{kk}^{20} & \underline{Z}_{kk}^{21} & \underline{Z}_{kk}^{22} \end{bmatrix}. \quad (20)$$

- Two-phase fault node k

$$\underline{Y}_L^F \underline{Y}_U^F \begin{bmatrix} \underline{Z}_{1k}^{00} & \underline{Z}_{1k}^{01} \\ \vdots & \vdots \\ \underline{Z}_{kk}^{00} & \underline{Z}_{kk}^{01} \\ \underline{Z}_{kk}^{10} & \underline{Z}_{kk}^{11} \\ \vdots & \vdots \\ \vdots & \vdots \end{bmatrix} = \begin{bmatrix} 0 & 0 \\ \vdots & \vdots \\ 1 & 0 \\ 0 & 1 \\ \vdots & \vdots \\ 0 & 0 \end{bmatrix} \quad (21)$$

$$\Rightarrow \underline{Z}_{Th-k}^{F_2} = \begin{bmatrix} \underline{Z}_{kk}^{00} & \underline{Z}_{kk}^{01} \\ \underline{Z}_{kk}^{10} & \underline{Z}_{kk}^{11} \end{bmatrix}. \quad (22)$$

- One-phase fault node k

$$\underline{Y}_L^F \underline{Y}_U^F [\underline{Z}_{1k}^{00} \cdots \underline{Z}_{kk}^{00} \cdots \underline{Z}_{nk}^{00}]^T = [0 \cdots 1 \cdots 0]^T \quad (23)$$

$$\Rightarrow \underline{Z}_{Th-k}^{F_1} = \underline{Z}_{kk}^{00}. \quad (24)$$

Step 4) Calculate the Fortescue fault currents and voltages from the boundary conditions and the Thévenin equivalent representation.

- Three-phase fault node k

$$\begin{bmatrix} \underline{Z}_{Th-k}^{F_3} & I_{3 \times 3} \\ \underline{C}_{I_{3\phi}} \underline{T}_{F_3}^{ph_3} & C_{V_{3\phi}} \underline{T}_{F_3}^{ph_3} \end{bmatrix} \begin{bmatrix} \underline{I}_k^{F_3} \\ \underline{V}_k^{F_3} \end{bmatrix} = \begin{bmatrix} \underline{V}_{Th-k}^{F_3} \\ 0 \end{bmatrix}. \quad (25)$$

- Two-phase fault node k

$$\begin{bmatrix} \underline{Z}_{Th-k}^{F_2} & I_{2 \times 2} \\ \underline{C}_{I_{2\phi}} \underline{T}_{F_2}^{ph_2} & C_{V_{2\phi}} \underline{T}_{F_2}^{ph_2} \end{bmatrix} \begin{bmatrix} \underline{I}_k^{F_2} \\ \underline{V}_k^{F_2} \end{bmatrix} = \begin{bmatrix} \underline{V}_{Th-k}^{F_2} \\ 0 \end{bmatrix}. \quad (26)$$

- One-phase fault node k

$$\begin{bmatrix} \underline{Z}_{Th-k}^{F_1} & 1 \\ \underline{C}_{I_{1\phi}} \underline{T}_{F_1}^{ph_1} & C_{V_{1\phi}} \underline{T}_{F_1}^{ph_1} \end{bmatrix} \begin{bmatrix} \underline{I}_k^{F_1} \\ \underline{V}_k^{F_1} \end{bmatrix} = \begin{bmatrix} \underline{V}_{Th-k}^{F_1} \\ 0 \end{bmatrix}. \quad (27)$$

Step 5) Calculate the Fortescue voltages at an arbitrary node i , while the fault is at node k . Node i can be of the three-phase ($p = 0, 1, 2$), two-phase ($p = 0, 1$) or one-phase ($p = 0$) type. The change in node voltages due to the fault current injections is computed using the Fortescue transfer impedances found in Step 3.

- Three-phase fault node k

$$\underline{V}_i^p = \underline{V}_{Th-i}^p - \sum_{q=0}^2 \underline{Z}_{ik}^{pq} \underline{I}_k^q, \quad p \in \{0, 1, 2\}. \quad (28)$$

- Two-phase fault node k

$$\underline{V}_i^p = \underline{V}_{Th-i}^p - \sum_{q=0}^1 \underline{Z}_{ik}^{pq} \underline{I}_k^q, \quad p \in \{0, 1, 2\}. \quad (29)$$

- One-phase fault node k

$$\underline{V}_i^p = \underline{V}_{Th-i}^p - \underline{Z}_{ik}^{p0} \underline{I}_k^0, \quad p \in \{0, 1, 2\}. \quad (30)$$

Given the branch model [20], the computation of the branch currents immediately follows in Fortescue and phase coordinates.

V. FAULT BOUNDARY CONDITIONS

This section describes the formation of the matrices ($\underline{C}_{I_{3\phi}}$, $C_{V_{3\phi}}$, $\underline{C}_{I_{2\phi}}$, $C_{V_{2\phi}}$, $\underline{C}_{I_{1\phi}}$, $C_{V_{1\phi}}$) that define the fault boundary conditions (13), (14), and (15). The use of the impedances \underline{Z}_f and \underline{Z}_g in defining these conditions follows the terminology in [1]. For illustration, Figs. 4–10 show diagrams for (4) an SLG fault at phase a of a three-phase node, (5) an LL fault between phases a - b of a three-phase node, (6) a 2LG fault between phases a - b of a three-phase node, (7) a 3-ph-G fault, (8) an SLG fault at phase x of a two-phase node ($xy \in \{ab, bc, ca\}$), (9) an LL fault in a two-phase node, and (10) a 2LG fault in a two-phase node.

A. Three-Phase Node Faults: $ph_3 = abc$

1) Single Line-to-Ground (SLG) Fault:

- SLG fault at phase a (see Fig. 4)

$$\underline{C}_{I_{3\phi}} = \begin{bmatrix} -\underline{Z}_f & 0 & 0 \\ 0 & 1 & 0 \\ 0 & 0 & 1 \end{bmatrix}; \quad C_{V_{3\phi}} = \begin{bmatrix} 1 & 0 & 0 \\ 0 & 0 & 0 \\ 0 & 0 & 0 \end{bmatrix}. \quad (31)$$

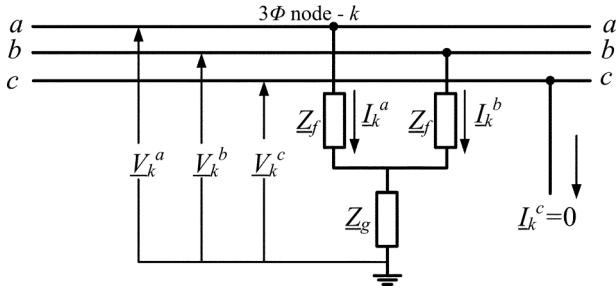


Fig. 6. 2LG fault between phases a-b of a three-phase node.

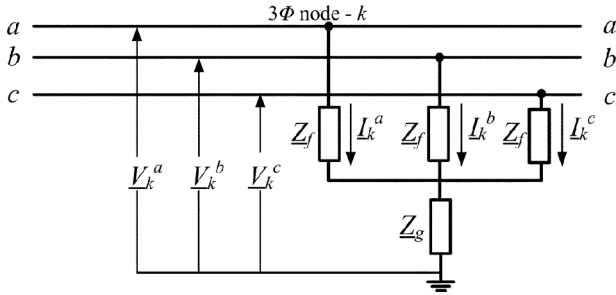


Fig. 7. 3-ph-G fault.

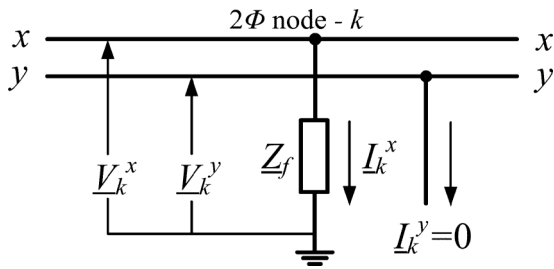


Fig. 8. SLG fault at phase x of a two-phase node.

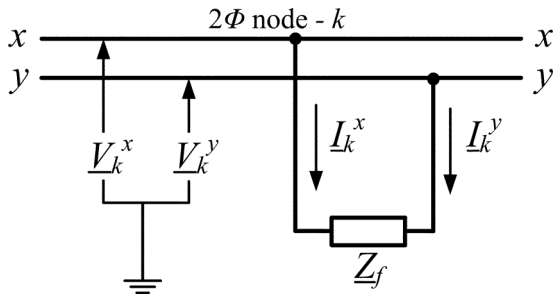


Fig. 9. LL fault in a two-phase node.

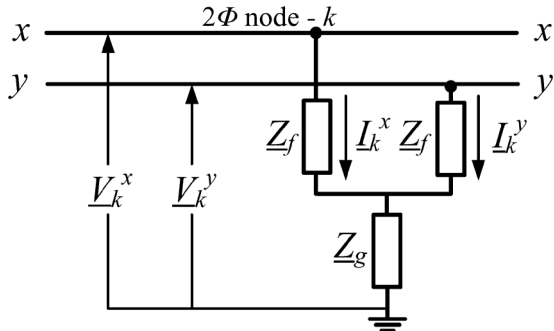


Fig. 10. 2LG fault in a two-phase node.

- SLG fault at phase b

$$\underline{C}_{I3\phi} = \begin{bmatrix} 1 & 0 & 0 \\ 0 & -\underline{Z}_f & 0 \\ 0 & 0 & 1 \end{bmatrix}; \quad C_{V3\phi} = \begin{bmatrix} 0 & 0 & 0 \\ 0 & 1 & 0 \\ 0 & 0 & 0 \end{bmatrix}. \quad (32)$$

- SLG fault at phase c

$$\underline{C}_{I3\phi} = \begin{bmatrix} 1 & 0 & 0 \\ 0 & 1 & 0 \\ 0 & 0 & -\underline{Z}_f \end{bmatrix}; \quad C_{V3\phi} = \begin{bmatrix} 0 & 0 & 0 \\ 0 & 0 & 0 \\ 0 & 0 & 1 \end{bmatrix}. \quad (33)$$

2) Line-to-Line (LL) Fault:

- LL Fault between phases a-b (see Fig. 5)

$$\underline{C}_{I3\phi} = \begin{bmatrix} 0 & 0 & 1 \\ 1 & 1 & 0 \\ -\underline{Z}_f & 0 & 0 \end{bmatrix}; \quad C_{V3\phi} = \begin{bmatrix} 0 & 0 & 0 \\ 0 & 0 & 0 \\ 1 & -1 & 0 \end{bmatrix}. \quad (34)$$

- LL Fault between phases b-c

$$\underline{C}_{I3\phi} = \begin{bmatrix} 1 & 0 & 0 \\ 0 & 1 & 1 \\ 0 & -\underline{Z}_f & 0 \end{bmatrix}; \quad C_{V3\phi} = \begin{bmatrix} 0 & 0 & 0 \\ 0 & 0 & 0 \\ 0 & 1 & -1 \end{bmatrix}. \quad (35)$$

- LL Fault between phases c-a

$$\underline{C}_{I3\phi} = \begin{bmatrix} 0 & 1 & 0 \\ 1 & 0 & 1 \\ 0 & 0 & -\underline{Z}_f \end{bmatrix}; \quad C_{V3\phi} = \begin{bmatrix} 0 & 0 & 0 \\ 0 & 0 & 0 \\ -1 & 0 & 1 \end{bmatrix}. \quad (36)$$

3) Double Line-to-Ground (2LG) Fault:

- 2LG Fault between phases a-b (see Fig. 6)

$$\underline{C}_{I3\phi} = \begin{bmatrix} 0 & 0 & 1 \\ -(\underline{Z}_f + \underline{Z}_g) & -\underline{Z}_g & 0 \\ -\underline{Z}_g & -(\underline{Z}_f + \underline{Z}_g) & 0 \end{bmatrix}; \quad C_{V3\phi} = \begin{bmatrix} 0 & 0 & 0 \\ 1 & 0 & 0 \\ 0 & 1 & 0 \end{bmatrix}. \quad (37)$$

- 2LG Fault between phases b-c

$$\underline{C}_{I3\phi} = \begin{bmatrix} 1 & 0 & 0 \\ 0 & -(\underline{Z}_f + \underline{Z}_g) & -\underline{Z}_g \\ 0 & -\underline{Z}_g & -(\underline{Z}_f + \underline{Z}_g) \end{bmatrix}; \quad C_{V3\phi} = \begin{bmatrix} 0 & 0 & 0 \\ 0 & 1 & 0 \\ 0 & 0 & 1 \end{bmatrix}. \quad (38)$$

- 2LG Fault between phases c-a

$$\underline{C}_{I3\phi} = \begin{bmatrix} 0 & 1 & 0 \\ -\underline{Z}_g & 0 & -(\underline{Z}_f + \underline{Z}_g) \\ -(\underline{Z}_f + \underline{Z}_g) & 0 & -\underline{Z}_g \end{bmatrix}; \quad C_{V3\phi} = \begin{bmatrix} 0 & 0 & 0 \\ 0 & 0 & 1 \\ 1 & 0 & 0 \end{bmatrix}. \quad (39)$$

4) Three-Phase (3-ph) Fault Without Ground Connection:

$$\underline{C}_{I3\phi} = \begin{bmatrix} 1 & 1 & 1 \\ -\underline{Z}_f & \underline{Z}_f & 0 \\ 0 & -\underline{Z}_f & \underline{Z}_f \end{bmatrix}; \quad C_{V3\phi} = \begin{bmatrix} 0 & 0 & 0 \\ 1 & -1 & 0 \\ 0 & 1 & -1 \end{bmatrix}. \quad (40)$$

5) *Three-Phase to Ground (3-ph-G) Fault (see Fig. 7):*

$$\underline{C}_{I3\phi} = \begin{bmatrix} -(\underline{Z}_f + \underline{Z}_g) & -\underline{Z}_g & -\underline{Z}_g \\ -\underline{Z}_g & -(\underline{Z}_f + \underline{Z}_g) & -\underline{Z}_g \\ -\underline{Z}_g & -\underline{Z}_g & -(\underline{Z}_f + \underline{Z}_g) \end{bmatrix};$$

$$C_{V3\phi} = \begin{bmatrix} 1 & 0 & 0 \\ 0 & 1 & 0 \\ 0 & 0 & 1 \end{bmatrix}. \quad (41)$$

B. *Two-Phase Node Faults: $ph_2 = xy \in \{ab, bc, ca\}$*

1) *Single Line-to-Ground (SLG) Fault:*

- SLG Fault at phase x (see Fig. 8)

$$\underline{C}_{I2\phi} = \begin{bmatrix} 0 & 1 \\ -\underline{Z}_f & 0 \end{bmatrix}; C_{V2\phi} = \begin{bmatrix} 0 & 0 \\ 1 & 0 \end{bmatrix}. \quad (42)$$

- SLG Fault at phase y

$$\underline{C}_{I2\phi} = \begin{bmatrix} 1 & 0 \\ 0 & -\underline{Z}_f \end{bmatrix}; C_{V2\phi} = \begin{bmatrix} 0 & 0 \\ 0 & 1 \end{bmatrix}. \quad (43)$$

2) *Line-to-Line (LL) Fault (see Fig. 9):*

$$\underline{C}_{I2\phi} = \begin{bmatrix} 1 & 1 \\ -\underline{Z}_f & 0 \end{bmatrix}; C_{V2\phi} = \begin{bmatrix} 0 & 0 \\ 1 & -1 \end{bmatrix}. \quad (44)$$

3) *Double Line-to-Ground (2LG) Fault (see Fig. 10):*

$$\underline{C}_{I3\phi} = \begin{bmatrix} -(\underline{Z}_f + \underline{Z}_g) & -\underline{Z}_g \\ -\underline{Z}_g & -(\underline{Z}_f + \underline{Z}_g) \end{bmatrix};$$

$$C_{V3\phi} = \begin{bmatrix} 1 & 0 \\ 0 & 1 \end{bmatrix}. \quad (45)$$

C. *One-Phase Node Fault: $ph_1 = x \in \{a, b, c\}$*

1) *Single Line-to-Ground (SLG) Fault:*

$$\underline{C}_{I1\phi} = -\underline{Z}_f; C_{V1\phi} = 1. \quad (46)$$

VI. DEMONSTRATION EXAMPLE

Consider the 4-node multiphase network shown in Fig. 11 having three lines; buses 1 and 2 are three-phase (abc) nodes, bus 3 is a two-phase (ab) node, and bus 4 is a single-phase (c) node. Consequently the line connecting bus 1 to bus 2 is three-phase, the line between bus 2 and bus 3 comprises only phases a and b , whereas the the line connecting bus 2 to bus 3 consists only of phase c . Equations (47), (48), and (49) respectively show the ordinary primitive admittance matrices for the three-phase, two-phase, and single-phase lines (in S); for simplicity, the lines are modeled without shunt charging effects:

$$\underline{Y}_{ph_3} = \begin{bmatrix} 0.354-1.128j & -0.087+0.317j & -0.087+0.317j \\ -0.087+0.317j & 0.354-1.128j & -0.087+0.317j \\ -0.087+0.317j & -0.087+0.317j & 0.354-1.128j \end{bmatrix} \quad (47)$$

$$\underline{Y}_{ph_2} = \begin{bmatrix} 0.411 - 0.377j & -0.137 + 0.056j \\ -0.137 + 0.056j & 0.411 - 0.377j \end{bmatrix} \quad (48)$$

$$\underline{Y}_{ph_1} = [0.368 - 0.378j]. \quad (49)$$

An LL Fault between phases a - b is simulated at bus 3 for the example in Fig. 11. For this example, the step-by-step procedure in Section IV is available as an electronic companion [24] which can be executed in the MATLAB environment; the details of this implementation are described below.

Step 1) This step requires forming the Fortescue nodal admittance matrix. Towards this end, the primitive \underline{Y}_{node} matrix corresponding to each of the three lines in Fig. 11 are formed:

- Three-phase (abc) line 1-2:

$$\underline{Y}_{1-2}^{F_3} = \begin{bmatrix} \underline{Y}_{1,1}^{F_3} & \underline{Y}_{1,2}^{F_3} \\ \underline{Y}_{2,1}^{F_3} & \underline{Y}_{2,2}^{F_3} \end{bmatrix} \quad (50)$$

$$\underline{Y}_{-1,1}^{F_3} = \underline{Y}_{2,2}^{F_3} = \underline{T}_{ph_3}^{F_3} \underline{Y}_{ph_3} \underline{T}_{F_3}^{ph_3}$$

$$= \begin{bmatrix} 0.180-0.493j & 0 & 0 \\ 0 & 0.441-1.445j & 0 \\ 0 & 0 & 0.441-1.445j \end{bmatrix} \quad (51)$$

$$\underline{Y}_{-1,2}^{F_3} = \underline{Y}_{2,1}^{F_3} = -\underline{Y}_{1,1}^{F_3}. \quad (52)$$

- Two-phase (ab) line 2-3, with a PTN connecting the $F_{3(ab)}$ and F_2 Fortescue domains [20]:

$$\underline{Y}_{2-3}^{F_3} = \begin{bmatrix} \underbrace{\underline{Y}_{2,2}^{F_{3(ab)}}}_{3 \times 3} & \underbrace{\underline{Y}_{2,3}^{F_3 \leftarrow F_2}}_{3 \times 2} \\ \underbrace{\underline{Y}_{3,2}^{F_2 \leftarrow F_3}}_{2 \times 3} & \underbrace{\underline{Y}_{3,3}^{F_2}}_{2 \times 2} \end{bmatrix} \quad (53)$$

$$\underline{Y}_{2,2}^{F_{3(ab)}} = \underline{T}_{ab}^{F_3} \underline{Y}_{2,2}^{ab} \underline{T}_{F_3}^{ab}$$

$$= \frac{1}{3} \begin{bmatrix} 1 & 1 & 1 \\ 1 & \underline{a}_3 & \underline{a}_3^2 \end{bmatrix}^T \underline{Y}_{ph_2} \begin{bmatrix} 1 & 1 & 1 \\ 1 & \underline{a}_3^2 & \underline{a}_3 \end{bmatrix}$$

$$= \begin{bmatrix} 0.182-0.214j & -0.047-0.132j & 0.138+0.025j \\ 0.138+0.025j & 0.319-0.270j & -0.027-0.279j \\ -0.047-0.132j & 0.255+0.116j & 0.319-0.270j \end{bmatrix} \quad (54)$$

$$\underline{Y}_{2,3}^{F_3 \leftarrow F_2} = \underline{T}_{ab}^{F_3} \underline{Y}_{2,3}^{ab} \underline{T}_{F_2}^{ab}$$

$$= \frac{1}{3} \begin{bmatrix} 1 & 1 & 1 \\ 1 & \underline{a}_3 & \underline{a}_3^2 \end{bmatrix}^T (-\underline{Y}_{ph_2}) \begin{bmatrix} 1 & 1 \\ 1 & -1 \end{bmatrix}$$

$$= \begin{bmatrix} -0.182 + 0.214j & 0 \\ -0.138 - 0.025j & -0.149 + 0.375j \\ 0.047 + 0.132j & -0.399 + 0.059j \end{bmatrix} \quad (55)$$

$$\underline{Y}_{3,2}^{F_2 \leftarrow F_3} = \underline{T}_{ab}^{F_2} \underline{Y}_{3,2}^{ab} \underline{T}_{F_3}^{ab}$$

$$= \frac{1}{2} \begin{bmatrix} 1 & 1 \\ 1 & -1 \end{bmatrix} (-\underline{Y}_{ph_2}) \begin{bmatrix} 1 & 1 & 1 \\ 1 & \underline{a}_3^2 & \underline{a}_3 \end{bmatrix}$$

$$= \begin{bmatrix} -0.273+0.321j & 0.071+0.199j & -0.207-0.038j \\ 0 & -0.599 + 0.088j & -0.223+0.562j \end{bmatrix} \quad (56)$$

$$\underline{Y}_{3,3}^{F_2} = \underline{T}_{ab}^{F_2} \underline{Y}_{3,3}^{ab} \underline{T}_{F_2}^{ab}$$

$$= \frac{1}{2} \begin{bmatrix} 1 & 1 \\ 1 & -1 \end{bmatrix} \underline{Y}_{ph_2} \begin{bmatrix} 1 & 1 \\ 1 & -1 \end{bmatrix}$$

$$= \begin{bmatrix} 0.273 - 0.321j & 0 \\ 0 & 0.548 - 0.433j \end{bmatrix}. \quad (57)$$

- Single-phase (c) line 2–4, with a PTN connecting the $F_{3(c)}$ and F_1 Fortescue domains [20]:

$$\underline{Y}_{2-4}^{F_3} = \begin{bmatrix} \underbrace{\underline{Y}_{2,2}^{F_{3(c)}}}_{3 \times 3} & \underbrace{\underline{Y}_{2,4}^{F_3 \leftarrow F_1}}_{3 \times 1} \\ \underbrace{\underline{Y}_{4,2}^{F_1 \leftarrow F_3}}_{1 \times 3} & \underbrace{\underline{Y}_{4,4}^{F_1}}_{1 \times 1} \end{bmatrix} \quad (58)$$

$$\begin{aligned} \underline{Y}_{2,2}^{F_{3(c)}} &= \underline{T}_c^{F_3} \underline{Y}_{2,2}^c \underline{T}_{F_3}^c \\ &= \frac{1}{3} [1 \quad \underline{a}_3^2 \quad \underline{a}_3]^T \underline{Y}_{ph_1} [1 \quad \underline{a}_3 \quad \underline{a}_3^2] \\ &= \begin{bmatrix} 0.123-0.126j & 0.048+0.169j & -0.17-0.043j \\ -0.17-0.043j & 0.123-0.126j & 0.048+0.169j \\ 0.048+0.169j & -0.17-0.043j & 0.123-0.126j \end{bmatrix} \end{aligned} \quad (59)$$

$$\begin{aligned} \underline{Y}_{2,4}^{F_3 \leftarrow F_1} &= \underline{T}_c^{F_3} \underline{Y}_{2,4}^c \underline{T}_{F_1}^c \\ &= \frac{1}{3} [1 \quad \underline{a}_3^2 \quad \underline{a}_3]^T (-\underline{Y}_{ph_1}) [1] \\ &= \begin{bmatrix} -0.123 + 0.126j \\ 0.170 + 0.043j \\ -0.048 - 0.169j \end{bmatrix} \end{aligned} \quad (60)$$

$$\begin{aligned} \underline{Y}_{4,2}^{F_1 \leftarrow F_3} &= \underline{T}_c^{F_1} \underline{Y}_{4,2}^c \underline{T}_{F_3}^c \\ &= [1] (-\underline{Y}_{ph_1}) [1 \quad \underline{a}_3 \quad \underline{a}_3^2] \\ &= [-0.368+0.378j \quad -0.143-0.51j \quad 0.51+0.13j] \end{aligned} \quad (61)$$

$$\begin{aligned} \underline{Y}_{4,4}^{F_1} &= \underline{T}_c^{F_1} \underline{Y}_{ph_1} \underline{T}_{F_1}^c \\ &= [1] \underline{Y}_{4,4}^c [1] \\ &= [0.368 - 0.378j]. \end{aligned} \quad (62)$$

The Fortescue equivalent nodal admittance matrix (in S) is then obtained using node overlapping:

$$\underline{Y}^F = \begin{bmatrix} I_{3 \times 3} & 0 & 0 & 0 \\ \underline{Y}_{2,1}^{F_3} & \underline{Y}_{2,2}^{F_3} + \underline{Y}_{2,2}^{F_{3(ab)}} + \underline{Y}_{2,2}^{F_{3(c)}} & \underline{Y}_{2,3}^{F_3 \leftarrow F_2} & \underline{Y}_{2,4}^{F_3 \leftarrow F_1} \\ 0 & \underline{Y}_{3,2}^{F_2 \leftarrow F_3} & \underline{Y}_{3,3}^{F_2} & 0 \\ 0 & \underline{Y}_{4,2}^{F_1 \leftarrow F_3} & 0 & \underline{Y}_{4,4}^{F_1} \end{bmatrix}. \quad (63)$$

- Step 2: To calculate the pre-fault or Thévenin voltage vector at bus 3, (64) is solved with the coefficient matrix given by (63):

$$\underline{Y}^F \underline{V}_{Th}^F = [V_{sl}^F \quad 0_{1 \times 3} \quad 0_{1 \times 2} \quad 0_{1 \times 1}]^T \quad (64)$$

where the slack (injection) voltage is given as a symmetric three phase line-to-neutral vector:

$$V_{sl}^{F_3} = [0 \quad 4160 \quad 0] \text{ V}. \quad (65)$$

After solving (64) for \underline{V}_{Th}^F , the Fortescue Thévenin voltage at node 3 can be extracted:

$$\underline{V}_{Th-3}^{F_2} = \underline{V}_{Th}^F(7:8) = \begin{bmatrix} 2080e^{-j60^\circ} \\ 3602.7e^{j30^\circ} \end{bmatrix} \text{ V}. \quad (66)$$

- Step 3: The Fortescue Thévenin impedance matrix at node 3 is obtained by solving:

$$\underline{Y}^F \underline{Z}_{Th}^F = I_{Th,rhs}^F \quad (67)$$

where

$$I_{Th,rhs}^F = \begin{bmatrix} 0_{6 \times 2} \\ I_{2 \times 2} \\ 0_{1 \times 2} \end{bmatrix} \quad (68)$$

and $I_{2 \times 2}$ is a two-by-two identity matrix. After solving (67) for \underline{Z}_{Th}^F , the Fortescue Thévenin impedance matrix (in Ω) at node 3 can be extracted:

$$\begin{aligned} \underline{Z}_{Th-3}^{F_2} &= \underline{Z}_{Th}^F(7:8, 1:2) \\ &= \begin{bmatrix} 2.036+3.209j & 0 \\ 0 & 1.316+1.521j \end{bmatrix}. \end{aligned} \quad (69)$$

The Fortescue Thévenin equivalent at node 3 is shown schematically in Fig. 12.

- Step 4: Substituting (36) with $Z_f = 0$ in (26) and solving gives

$$\underline{I}_{fault-3}^{F_2} = \begin{bmatrix} 0 \\ 1791.3e^{-j19.14^\circ} \end{bmatrix} \text{ A} \quad (70)$$

$$\underline{V}_{fault-3}^{F_3} = \begin{bmatrix} 2080e^{-j60^\circ} \\ 0 \end{bmatrix} \text{ V} \quad (71)$$

or in phase coordinates

$$\underline{I}_{fault-3}^{(ab)} = \begin{bmatrix} 1791.3e^{-j19.14^\circ} \\ 1791.3e^{j160.86^\circ} \end{bmatrix} \text{ A} \quad (72)$$

$$\underline{V}_{fault-3}^{(ab)} = \begin{bmatrix} 2080e^{-j60^\circ} \\ 2080e^{-j60^\circ} \end{bmatrix} \text{ V}. \quad (73)$$

- Step 5: The Fortescue transfer impedance (in Ω) for node 4 is

$$\underline{Z}_{transf-4}^{F_2} = \underline{Z}_{Th}^F(9, 1:2) = [0.307 + 0.770j \quad 0]. \quad (74)$$

The Fortescue pre-fault voltage at node 4:

$$\underline{V}_{Th-4}^0 = \underline{V}_{Th-4}^{F_1} = \underline{V}_{Th}^F(9) = 4160e^{j120^\circ} \text{ V}. \quad (75)$$

Using (29) gives

$$\begin{aligned} \underline{V}_{fault-4}^0 &= \underline{V}_{Th-4}^0 - \underline{Z}_{transf-4}^{F_2} \underline{I}_{fault-3}^{F_2} \\ &= 4160e^{j120^\circ} \text{ V}. \end{aligned} \quad (76)$$

This is an expected result since phase c at node 4 was not affected by the LL fault at node 3.

VII. NUMERICAL RESULTS

The Fortescue SCC approach was tested on three standard test feeders (IEEE 13-node, IEEE 34-node, IEEE 123-node) in addition to four practical test networks having 1505, 2986, 8500, and 14 200 nodes; it was compared with an implementation of the classical canonical SCC method in phase coordinates [7], where the unity current injection method was used in computing the

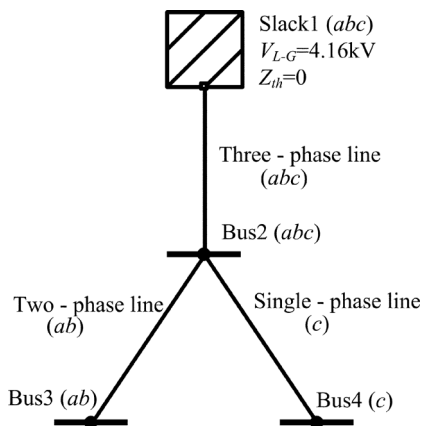


Fig. 11. 4-node multiphase network.

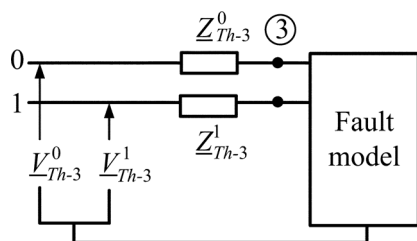


Fig. 12. Fortescue Thévenin equivalent at node 3.

Thévenin impedance matrix and the post-fault voltage vector [4]. Distributed loads were modeled by two spot loads at each end of the line following the approach in [14]. Tests were conducted for SLG, 2L, 2LG, 3-ph, and 3-ph-G faults; the SCC approaches operating in Fortescue and phase coordinates gave virtually identical results when viewed in the same domain, thus confirming the correctness of the implementations. The main advantage of the Fortescue approach is in the computational speed-up, which is particularly important for real-time applications as discussed in Section II. Table I presents performance test results on four large networks, showing that the Fortescue approach requires between 34% and 56% of the execution time in phase coordinates. The speed-up is affected by the proportion of branches that are connected to PTNs; in fact the largest speed-up is for Net. IV, which is a European urban distribution network with few laterals having less than three phases. The execution time in this table includes one LU factorization step, one forward/backward substitution for computing the pre-fault voltages, and two forward/backward substitutions for the Thévenin equivalent matrix calculation (faults are simulated on two-phase nodes). All implementations were programmed in C++ using an in-house developed sparse matrix library, and the computations were carried out on a high-performance PC (Intel i7–2600 K, 8 GB RAM). The computational time of SCC is mainly consumed in the LU decomposition of the nodal admittance matrix and the forward/backward substitutions; the implementation of these tasks in both Fortescue and phase coordinates makes use of an industrial grade software developed for the implicit Z-bus power flow [20]. The improved computational performance on practical distribution networks is attributed to the higher degree of decoupling in the Fortescue nodal admittance matrix as compared to the phase coordinates nodal admittance matrix.

TABLE I
PERFORMANCE TEST RESULTS (2LG FAULTS)

Test network	No. of buses	Branches with PTNs [%] (unsymmetry)	Execution time in phase coord. T_{ph} [ms]	Execution time in Fortescue coord. T_F [ms]	Calculation time reduction T_F/T_{ph}
Net. I	1505	19	87.05	48.75	0.56
Net. II	2986	20	172.14	94.67	0.55
Net. III	8500	9	375.97	169.19	0.45
Net. IV	14200	< 1	939.06	319.28	0.34

VIII. CONCLUSION

Distribution system applications in smart networks require real-time computations to support automation. Functions that are influenced by distribution protection, such as feeder reconfiguration, demand real-time fault analysis which is oriented towards network operation rather than planning; this makes computing time a major concern in real-time SCC. This paper proposes a multiphase SCC approach that operates in Fortescue coordinates, and builds on recent developments in Fortescue-based distribution system power flow. The proposed approach shows significant computational improvement over the classical phase coordinates method.

REFERENCES

- [1] P. M. Anderson, *Analysis of Faulted Power Systems*. New York, NY, USA: IEEE Press, 1995.
- [2] C. L. Fortescue, "Method of symmetrical co-ordinates applied to the solution of polyphase networks," *Trans. AIEE*, vol. XXXVII, no. 2, pp. 1027–1140, Jul. 1918.
- [3] X. Zhang, F. Soudi, D. Shirmohammadi, and C. S. Cheng, "A distribution short circuit analysis approach using hybrid compensation method," *IEEE Trans. Power Syst.*, vol. 10, no. 4, pp. 2053–2059, Nov. 1995.
- [4] T.-H. Chen, M.-S. Chen, W.-J. Lee, P. Kotas, and P. V. Olinda, "Distribution system short circuit analysis—a rigid approach," *IEEE Trans. Power Syst.*, vol. 7, no. 1, pp. 444–450, Feb. 1992.
- [5] M. A. Laughton, "Analysis of unbalanced polyphase networks by the method of phase co-ordinates—part 1: System representation in phase frame of reference," *Proc. IEE*, vol. 115, no. 8, pp. 1163–1172, Aug. 1968.
- [6] M. A. Laughton, "Analysis of unbalanced polyphase networks by the method of phase co-ordinates. Part 2: Fault analysis," *Proc. IEE*, vol. 116, no. 5, pp. 857–865, May 1969.
- [7] V. C. Strezoski and D. D. Bekut, "A canonical model for the study of faults in power systems," *IEEE Trans. Power Syst.*, vol. 6, no. 4, pp. 1493–1499, Nov. 1991.
- [8] W. H. Kersting and W. H. Phillips, "Distribution system short circuit analysis," in *Proc. 25th Intersociety Energy Conversion Eng. Conf. (IECEC-90)*, Aug. 1990, vol. 1, pp. 310–315.
- [9] W. H. Kersting, *Distribution system modeling and analysis*. Boca Raton, FL, USA: CRC Press, 2002.
- [10] M. P. Selvan and K. S. Swarup, "Unbalanced distribution system short circuit analysis—an object-oriented approach," in *Proc. IEEE Region 10 Conf. (TENCON 2008)*, Nov. 2008, pp. 1–6.
- [11] A. Berman and W. Xu, "Analysis of faulted power systems by phase coordinates," *IEEE Trans. Power Del.*, vol. 13, no. 2, pp. 587–595, Apr. 1998.
- [12] P. A. N. Garcia, J. L. R. Pereira, M. P. Vinagre, and E. J. Oliveira, "Fault analysis using continuation power flow and phase coordinates," in *Proc. IEEE Power Eng. Soc. General Meeting*, Jun. 2004, pp. 872–874.
- [13] P. A. N. Garcia, J. L. R. Pereira, S. Carneiro, V. M. d. Costa Jr., and N. Martins, "Three-phase power flow calculations using the current injection method," *IEEE Trans. Power Syst.*, vol. 15, no. 2, pp. 508–514, May 2000.

- [14] C. S. Cheng and D. Shirmohammadi, "A three-phase power flow method for real-time distribution system analysis," *IEEE Trans. Power Syst.*, vol. 10, no. 2, pp. 671–679, May 1995.
- [15] J.-H. Teng, "Systematic short-circuit-analysis method for unbalanced distribution systems," *IEE Proc.-Gener. Transm. Distrib.*, vol. 152, no. 4, pp. 549–555, Jul. 2005.
- [16] J.-H. Teng, "Unsymmetrical short-circuit fault analysis for weakly meshed distribution systems," *IEEE Trans. Power Syst.*, vol. 25, no. 1, pp. 96–105, Feb. 2010.
- [17] W.-M. Lin and T.-C. Ou, "Unbalanced distribution network fault analysis with hybrid compensation," *IET Gener. Transm. Distrib.*, vol. 5, no. 1, Jan. 2011.
- [18] R. M. Ciric, L. F. Ochoa, A. Padilla-Feltrin, and H. Nouri, "Fault analysis in four-wire distribution networks," *IEE Proc.-Gener. Transm. Distrib.*, vol. 152, no. 6, pp. 977–982, Nov. 2005.
- [19] M. Abdel-Akher and K. M. Nor, "Fault analysis of multiphase distribution systems using symmetrical components," *IEEE Trans. Power Del.*, vol. 25, no. 4, pp. 2931–2939, Oct. 2010.
- [20] I. Džafić, B. C. Pal, M. Gilles, and S. Henselmeyer, "Generalized π Fortescue equivalent admittance matrix approach to power flowsolution," *IEEE Trans. Power Syst.*, vol. 29, no. 1, pp. 193–202, Jan. 2014.
- [21] I. Džafić, H.-T. Neisius, M. Gilles, S. Henselmeyer, and V. Landerberger, "Three-phase power flow in distribution networks using Fortescue transformation," *IEEE Trans. Power Syst.*, vol. 28, no. 2, pp. 1027–1034, May 2013.
- [22] F. L. Alvarado, "Formation of Y-node using the primitive Y-node concept," *IEEE Trans. Power App. Syst.*, vol. PAS-101, no. 12, pp. 4563–4571, Dec. 1982.
- [23] S. C. Chapra and R. P. Canale, *Numerical Methods for Engineers*, 2nd ed. Singapore: McGraw-Hill, 1988.
- [24] Matlab demonstration example for SCC in Fortescue coordinates accessed: 2014-10-14 [Online]. Available: https://dl.dropboxusercontent.com/u/47198710/SCC_Example.zip

Rabih A. Jabr (M'02–SM'09) was born in Lebanon. He received the B.E. degree in electrical engineering (with high distinction) from the American University of Beirut, Beirut, Lebanon, in 1997 and the Ph.D. degree in electrical engineering from Imperial College London, London, U.K., in 2000.

Currently, he is a Professor in the Department of Electrical and Computer Engineering at the American University of Beirut. His research interests are in mathematical optimization techniques and power system analysis and computing.

Izudin Džafić (M'05–SM'13) received the Ph.D. degree from the University of Zagreb, Croatia, in 2002.

He is currently an Associate Professor in the Department of Electrical Engineering at the International University of Sarajevo, Bosnia. From 2002 to 2014, he was with Siemens AG, Nuremberg, Germany, where he held the position of the Head of the Department and Chief Product Owner (CPO) for Distribution Network Analysis (DNA) R&D. His research interests include power system modeling, development and application of fast computing to power systems simulations.

Dr. Džafić is a member of the IEEE Power and Energy Society and the IEEE Computer Society.